Published in final edited form as:
J Neurophysiol. 2006 December ; 96(6): 3194–3208.

Properties of a Population of GABAergic Cells in Murine Auditory Cortex Weakly Excited by Thalamic Stimulation

Yakov I. Verbny[1], **Ferenc Erdélyi**[2], **Gábor Szabó**[2], and **Matthew I. Banks**[1]
1*Department of Anesthesiology, University of Wisconsin, Madison, Wisconsin;*

2*Department of Gene Technology and Developmental Neurobiology, Institute of Experimental Medicine, Budapest, Hungary*

Abstract

Feedforward inhibition triggered by thalamocortical (TC) afferents sharpens onset responses and shapes receptive fields of pyramidal cells in auditory cortex (ACx). Previous studies focused only on interneurons located in and around layer IV in primary ACx, target of the dense thalamic projections from ventral medial geniculate. We investigated a population of feedforward interneurons located throughout layers I-V and activated by both afferents from primary and nonprimary thalamus using recordings from auditory TC brain slices obtained from mice expressing green fluorescent protein under control of the glutamic acid decarboxylase (GAD65) promoter in a subpopulation of cortical GABAergic cells. We studied the responses of these interneurons and of pyramidal cells in ACx to thalamic stimulation and to hyper- and depolarizing current pulses. Most interneurons exhibited monosynaptic responses to thalamic stimulation, but this excitation was weak and subthreshold. Interneurons had multipolar dendritic morphology with widespread and dense axonal projections extending several hundred micrometers from the soma. In pyramidal cells from layers II-IV, thalamic excitatory postsynaptic potentials were significantly larger than in interneurons and were superthreshold in 40% of cells, but in these cells, there was no evidence of feedforward inhibition. By contrast, feedforward inhibition was observed in 12 of 18 layer V pyramidal cells. Thus feedforward inhibition in supragranular layers of ACx is weak, and these interneurons require coincident excitation to be activated by thalamic inputs.

INTRODUCTION

GABAergic interneurons play a critical role in regulating the activity of cortical pyramidal cells. These cells form a complex population that can be classified based on morphological, electrophysiological, and immunocytochemical properties (Connors and Gutnick 1990; Defelipe 1997; Markram et al. 2004). In sensory neocortex, at least some interneurons are directly excited by thalamic afferents, triggering short-latency feedforward inhibition in pyramidal cells that limits the temporal and spatial spread of excitation (White and Keller 1987). Identifying the interneurons targeted by thalamic afferents and the synaptic physiology of this connection is critical to understanding cortical sensory information processing.

Address for reprint requests and other correspondence: Matthew I. Banks, Dept of Anesthesiology, University of Wisconsin, 1300 University Ave., Room 4605, Madison, WI 53706 (E-mail: mibanks@wisc.edu)..

GRANTS
This work was supported by National Institute of Deafness and Other Communication Disorders Grant DC-006013 to M. I. Banks and the Department of Anesthesiology, University of Wisconsin, Madison, WI.

The costs of publication of this article were defrayed in part by the payment of page charges. The article must therefore be hereby marked "*advertisement*" in accordance with 18 U.S.C. Section 1734 solely to indicate this fact.

In auditory cortex (ACx), GABAergic inhibition serves to sharpen onset responses and shape the receptive field properties of pyramidal cells (Foeller et al. 2001; Muller and Scheich 1988; Wang et al. 2000). Inhibitory cells in ACx are excited by thalamocortical (TC) afferents (Cipolloni and Keller 1989; Mitani et al. 1985; Rose and Metherate 2005). This excitation likely triggers periods of inhibition in pyramidal cells after onset responses to acoustic stimuli in vivo and after electrical stimulation of thalamic afferents in vitro (Cruikshank et al. 2002; Hefti and Smith 2000; Volkov and Galazjuk 1991).

In primary ACx and somatosensory cortex, thalamic afferents terminate most densely in layer IV and adjacent areas of layer III (Lorente De No 1992). Studies of feedforward interneurons have invariably focused on cells located in these layers and have identified several populations of interneurons, e.g., fast spiking (FS) cells, that are strongly excited by thalamic afferents (Agmon and Connors 1992; Gibson et al. 1999; Porter et al. 2001; Rose and Metherate 2005). The FS cell population partially overlaps the population of parvalbuminpositive interneurons, which are thought be a major target of thalamic afferents in sensory neocortex (Staiger et al. 1996). However, thalamic afferents to sensory neocortex terminate in more superficial layers as well (Jones 1998), and the properties of feedforward interneurons in these layers have not been described previously.

As for other sensory modalities, the ascending auditory pathway can be divided into two parallel projections, the lemniscal and extralemniscal paths (Lorente De No 1938; Hu 2003; Jones 1998). The lemniscal pathway carries specific, sharply tuned, and temporally precise information from the ventral division of the medial geniculate body (vMGB) to layers III and IV in primary ACx (Lorente De No 1938). It is these fibers that excite the feedforward interneurons in layers III-V that have been the focus of previous reports in primary ACx and somatosensory cortex (Agmon and Connors 1992; Rose and Metherate 2005). In the auditory lemnsical pathway, vMGB projects almost exclusively to layers III and IV of primary ACx, and these layers of primary ACx receive all of their thalamic input from vMGB (Kimura et al. 2003; Roger and Arnault 1989; Scheel 1988). The one exception to this exclusive relationship is that these thalamic afferents can have collateral branches that terminate in more superficial layers of primary ACx, most densely in layer I (Cetas et al. 1999) where they may contact more superficial interneurons. The extralemniscal pathway carries less precisely tuned and timed information that may instead be important for polysensory integration and learning (Hu 2003). The extralemniscal pathway originates in nonprimary thalamic nuclei including the dorsal and medial divisions of the medial geniculate as well as several nuclei ventral and medial to the medial geniculate, including the posterior intralaminar and peripeduncular nuclei. This pathway terminates diffusely in primary and higher order ACx, but in primary ACx, terminals are restricted to layer I and to a lesser extent layer VI (Kimura et al. 2003; Linke and Schwegler 2000; Lorente De No 1938). Thus both the lemniscal and extralemniscal pathways have the potential to activate interneurons in areas outside of the classical thalamorecipient layers.

We adapted two recently developed techniques to enable us to study feedforward interneurons in auditory cortex in murine brain slices. The auditory thalamocortical (TC) slice preparation (Cruikshank et al. 2002), in which connections between the auditory thalamus and ACx remain intact, allowed us to study the properties of feedforward inhibition selectively (Agmon and Connors 1992; Rose and Metherate 2005). In this preparation, two slices are typically extracted from one animal: a "primary " slice, containing mostly vMGB and primary ACx, and a "shell" slice containing mostly nonprimary thalamic nuclei ventral to vMGB and secondary ACx ventral to primary ACx (Cruikshank et al. 2002). By definition, cells located outside of primary auditory cortex and activated by thalamic afferents are part of the extralemniscal pathway, and these cells will be most heavily represented in the shell slices. In primary ACx, cells located outside of layers I and VI that have dendrites in layers III and IV are most likely part of the lemniscal pathway due to the relatively exclusive connectivity between vMGB and layers III-

IV of primary ACx, and these cells will be most heavily represented in primary slices. We prepared auditory TC slices from mice genetically engineered to express green fluorescent protein in a subpopulation of GABAergic interneurons in neocortex (Lopez-Bendito et al. 2004), allowing us to target interneurons selectively and to study a specific subpopulation of GABAergic cells. These cells are located primarily in layers I-V and include most of the cells expressing cholecystokinin but rarely those expressing parvalbumin. The synaptic responses of these cells to thalamic stimulation have not previously been reported.

We found that most interneurons studied were directly activated by thalamic inputs, but the strength of this excitation was weak and almost always subthreshold. Feedforward interneurons had widespread axonal projections and could occur in layers I-V in both primary and shell slices. In contrast to interneurons, thalamic excitation in pyramidal cells was strong and often superthreshold. No evidence of disynaptic inhibition was observed in either interneurons or layer II-IV pyramidal cells. Feedforward inhibition in layer V pyramidal cells was observed in the majority of cells. These data suggest that feedforward inhibition in layers II-IV is weak and that interneurons in layers I-V require coincident excitation from other sources, e.g., cortical feedback or subcortical neuromodulators, to become activated. Because thalamic excitation was nearly always subthreshold in the interneurons studied here, feedforward inhibition observed in layer V pyramidal cells is likely mediated by interneurons that do not express the GAD65-eGFP transgene.

METHODS

Experimental animals

All experimental protocols conformed to APS/National Institutes of Health guidelines and were approved by the University of Wisconsin (UW) Research Animal Resources Committee. All experimental protocols conformed to APS/National Institutes of Health guidelines and were approved by the UW Research Animal Resources Committee. For this study, heterozygous transgenic mice on C56Bl6 background were used from line GAD65_3e/gfp5.5 #30 obtained from G. Szabo and colleagues (Lopez-Bendito et al. 2004). This transgenic line carries the egfp marker gene fused in frame with the third exon of the GAD65 gene. The transgenic construct contains the 5.5-kb form of the 5′-upstream region of the mouse GAD65 gene and the first three exons with introns 1 and 2 in between. The transgene-encoded protein is a fusion protein between 87 N-terminal amino acids from GAD65 and eGFP. Transgene expression has been shown to be exclusively neuronal and almost fully GABAergic. (Lopez-Bendito et al. 2004). The expression is partial but specific in almost all brain regions including the neocortex. Transgenic pups were selected based on green fluorescence visualized through the skull in neonates using a special goggle with built in GFP filter and light manufactured by BLS, Ltd (model GFsP-5; Budapest; www.bls-ltd.com).

Cells in slices obtained from transgenic animals displayed no adverse effects of the expression of GFP; for example, we observed no aggregation of GFP, no evidence of GFP toxicity-induced apoptosis or any kinds of morphological alterations in any brain regions. This is consistent with previous reports using these and other strains of GAD 65-eGFP transgenic animals that have found no evidence for developmental abnormalities, abnormal levels of apoptosis in interneurons, or abnormal electrophysiological or synaptic properties (Galarreta et al. 2004; Lopez-Bendito et al. 2004; Meyer et al. 2002; Oliva et al. 2000). Cells expressing GFP in our experiments had healthy resting potentials, fired large-amplitude action potentials with overshooting afterhyperpolarizations, and produced stable patch-clamp recordings that frequently lasted an hour or more. In addition, we compared the intrinsic properties of 13 layer I cells recorded in transgenic animals with those of 130 layer I cells from wild-type litter mates used for other experiments, and found no differences between these two groups (see RESULTS).

Slice preparation

Male and female mice [P13-P25; 17.0 ± 3.2 (SD) days old] were decapitated under isoflurane anesthesia, and the brain was extracted and immersed in artificial cerebrospinal fluid [ASCF, composition (in mM): 126 NaCl, 26 $NaHCO_3$, 1.8 KCl, 2.1 $CaCl_2$, 1.4 $MgSO_4$, 1.2 KH_2PO_4, and 10 glucose] at ~4°C. Thalamocortical (TC) slices (500 μm) were obtained as described (Cruikshank et al., 2002). Primary and shell slices were distinguished based on visual inspection during the slicing procedure. In primary slices, the hippocampus was elongated rostrocaudally, the fimbria/fornix was present, and the lateral and medial geniculate nuclei were clearly visible. Shell slices were identified as the next slice ventrally to the primary slice. In shell slices, the hippocampus was not elongated and the primary thalamic nuclei were not visible. Slices were maintained in ACSF saturated with 95% O_2-5% CO_2 at 24°C >1 h before transfer to the recording chamber, which was perfused at 3 ml/min with ACSF at 34°C.

Patch-clamp electrophysiology

Whole cell recordings were obtained at 34°C from interneurons and pyramidal cells located in layers I-V and visualized using a video camera (VE-1000; DAGE MTI, Michigan City, IN) connected to an upright microscope (BX-50WI; Olympus America, Melville, NY) equipped with an infrared band-pass filter (775 ± 75 nm), a long working-distance water-immersion objective (Olympus ×40, N.A. 0.7) and differential interference contrast optics. The microscope and recording pipette were under remote control using an integrated motorized control system (Luigs and Neumann, Ratingen, Germany). Patch pipettes were fabricated from borosilicate glass (KG-33, 1.7 mm OD, 1.1 mm ID; Garner Glass, Claremont, CA) using a Flaming-Brown two-stage puller (P-87; Sutter Instruments, Novato, CA). Patch pipettes had open-tip resistances of 4-6 MΩ. All pipettes contained 0.3% biocytin for cell staining. Current-clamp recordings were obtained with patch pipettes containing (in mM) 140 K-gluconate, 10 NaCl, 10 HEPES, 0.1 EGTA, and 2 MgATP, pH = 7.2. Data were amplified, low-pass filtered (10 kHz; Multiclamp 7A, Molecular Devices, Sunnyvale, Ca), digitized (20 kHz; DigiData 1322A, Molecular Devices), and recorded using pCLAMP v8.2 (Molecular Devices). Thalamic afferents were activated by stimulating in the superior thalamic radiation, mid-way between the medial geniculate and ACx, just rostral to the hippocampus, using bipolar tungsten electrodes. Cells were labeled with biocytin and slices were fixed in 4% paraformaldehyde for >24 h, usually 1-2 wk.

Tissue processing

Slices were processed over three days for biocytin staining as whole-mounts, i.e., without resectioning. Fixed slices were washed for 30 min in 0.01M phosphate buffered saline (PBS), then 15 min in 1.5% H_2O_2 in PBS, then 30 min again in 0.01M PBS. Slices were then rinsed for 30 min in 4% Triton-X and 1% bovine serum albumin (BSA) in PBS, and incubated overnight in the secondary antibody to the avidin-biotin-HRP complex (ABC Kit, Vector Labs) in PBS with 4% Triton-X and 1% BSA. On the second day, the slices were rinsed in 0.1 M PBS, the HRP was reacted using 0.04% diaminobenzidine with 0.01% H_2O_2 in 0.1 M PBS for 10 min, then the slices were rinsed for 40 min in PBS and kept in the refrigerator overnight. On the third day, we applied a silver/gold intensification procedure (entirely in the dark and at room temperature unless indicated otherwise) as follows. Slices were washed for 40 min in sterile deionized water (dH_2O), then incubated for 1h in 1.42% $AgNO_3$ at 56°C and washed in dH_2O for 40 min. Slices were then immersed in 5% $Na_2S_2O_3$ in dH_2O for 10 min, rinsed for 40 min in dH_2O and incubated in 0.2% $HAuCl_4$ for 30 min. Slices were then rinsed for 10 min in dH_2O and incubated again in 5% $Na_2S_2O_3$ in dH_2O for 10 min, and finally rinsed for 40 min in dH_2O. Finally the slices were mounted using Vectashield H-1000 mounting medium (Vector Labs, Burlingame, CA) and coverslipped. The stained cells were drawn by hand using a camera lucida attached to a Nikon upright microscope with ×100 oil-immersion objective.

Drawings were cut into 12 × 17-in sections, digitized at 600 dpi and reassembled in Adobe Photoshop. All chemicals were obtained from Sigma-Aldrich (Saint Louis, MO).

Histological analysis

For each labeled cell, we measured the distance from the pial surface to the position of the cell body and normalized this distance to the total distance from the pial surface to the white matter to yield the fractional depth [$d_{frac} \in (0,1)$] of each cell. For cells the axonal processes of which were well labeled, the horizontal (i.e., rostrocaudal) and vertical (i.e., mediolateral) spatial extent of axonal projections were measured in digitized camera lucida drawings in Adobe Photoshop, and the total area of axonal arbor was quantified as the product of these two factors. It should be noted that in three cases (but not in the cells illustrated in Figs. 6 and 7), the axon appeared to have been cut during the slicing procedure (based on the presence of a retraction bulb in the stained tissue), and thus these estimates should be considered to be lower bounds. To estimate the density of synaptic boutons in these digitized drawings, the number of swellings were counted in three identically sized rectangular regions, selected at random but with the following constraints: one region included the cell body, one was away from the cell body but within the same cortical layer as the cell body, and one was in an adjacent cortical layer to the cell body. These three counts were averaged, divided by the area of the rectangular search window and then by the thickness of the slice (500 μm) to yield a density measurement. This procedure was repeated three times with randomly selected search regions, and the density was estimated as the average of the three counts.

Electrophysiological data analysis

Evoked synaptic responses were analyzed using Clampfit (v9.2; Molecular Devices). Excitatory postsynaptic potentials (EPSPs) were characterized by their maximal subthreshold amplitude (A_{EPSP}) and duration at half-maximal amplitude ($t_{HW,\ EPSP}$), and the mean, SD and coefficient of variation of response latency (Lat_{Mn}, Lat_{SD}, Lat_{CV}), defined as the time from onset of the stimulus to the time the response rose from baseline to 10% of its peak amplitude. For each cell, we checked for the presence of inhibition, either by holding the cell at membrane potentials hyperpolarized and depolarized to rest or by holding the cells at a single potential depolarized to the chloride reversal potential (E_{Cl} =-68 mV).

Membrane and firing properties were measured using custom software written in Matlab v7.2 (Mathworks, Natick, MA) that extracted measurements from responses to 250-ms hyper- and depolarizing current pulses recorded under current clamp. The input resistance of the cell (R_{IN}) was estimated from the slope of the current-clamp current-voltage relationship for hyperpolarizing pulses measured using the peak voltage value during the response. The ratio of this slope to the slope measured from the voltage value at the end of the pulse (I-$V_{Slope\ ratio}$) was used to assess the magnitude of the hyperpolariza-tion activated cation current (I_h) in these cells (Banks et al. 1993). The resting membrane time constant (τ_{mem}) was estimated from the best single-exponential fit to the response to the smallest hyperpolarizing current pulse. From responses to superthreshold depolarizing current pulses, a current-spike frequency relationship (I-f curve) was measured and parameterized by its mean slope (I-f_{Slope}). Spike frequency adaptation was measured as the ratio of the first to last interspike interval during a 250-ms pulse eliciting a 25-Hz spike train (ISI_{ratio}). Spike threshold was measured as the membrane potential prior to a spike at which the first derivative of the membrane potential trace increased by fourfold relative to its mean value during the second half of the previous interspike interval. Spike shape was parameterized by measuring mean spike amplitude (A_{Spk}) and mean spike duration at half-amplitude ($t_{HW,\ spk}$) were measured for each current pulse eliciting spikes. The spike afterhyperpolarization (AHP) was analyzed by measuring its amplitude (A_{AHP}) and the time of its peak relative to the interspike interval [$t_{Pk,\ AHP} \in (0,1)$; e.g., a value of 0.1 means the AHP reached its peak 10 ms into an interspike interval of 100

ms]. Parameter values for firing properties are the means averaged over all spikes during the response to the current pulse eliciting a train of spikes at a spike frequency closest to 25 Hz in that cell.

All of the intrinsic properties were heterogeneous for interneurons. We attempted to classify interneurons according to these intrinsic properties using several methods but could find no quantitative, objective way to do this. For example, none of the parameters' measured distributions were multimodal, suggesting that based on single parameters cells did not readily divide into groups. Although there were significant correlations between some of the intrinsic parameters and synaptic parameters, these correlations appeared to represent continua rather than clusters of similar cells. Similarly, cluster analyses using all or a subset of the measured intrinsic and synaptic parameters yielded inconclusive results (not shown).

Statistical analysis

All data are presented as means ± SD. Statistical analysis was performed using SPSS v12.0 (SPSS, Chicago, IL). To determine statistical differences between means of parameter distributions, Student's *t*-test were used for pairwise comparisons. For comparisons across three or more groups, ANOVA was used with the Bonferroni post hoc test (used when variances were homogeneous across the groups) or Dunnett's T3 post hoc test (used when variances were not homogeneous across groups). The effects of age on synaptic and intrinsic properties was assessed first using multivariate linear regression with age as the independent variable and Lat_{Mn}, A_{EPSP}, $t_{HW,\ EPSP}$, τ_{mem}, R_{IN}, $I\text{-}V_{Slope\ ratio}$, V_{Thresh}, $I\text{-}f_{Slope}$, ISI_{Ratio}, A_{Spk}, $t_{HW,\ spk}$, A_{AHP}, and $t_{pk,\ AHP}$ as dependent variables. In this analysis cell type was not treated as an independent variable, i.e., data from all cell types were grouped together. To determine whether there were any differences in the effects of age depending on the cell type, we analyzed the data using the general linear model in SPSS with cell type as a fixed factor and age as a covariate. This is equivalent to a multivariate linear regression with age and cell type as independent variables. A third independent variable, an interaction term between age and cell type, was added to the model to capture any differential effects of age according to cell type.

RESULTS

Comparison of intrinsic properties in transgenic versus wild-type animals

We saw no evidence of developmental abnormalities, GFP-induced toxicity or any signs of unhealthy neurons in transgenic animals, indicating that the transgene itself had no influence on the properties of cells presented here. As an additional check, we compared the intrinsic properties of 13 layer I cells recorded from transgenic animals with those of 130 layer I cells from wild-type mice used for other experiments. The cells from transgenic animals include eight putative feedforward interneurons recorded in layer I the synaptic response properties of which are presented in the following text in detail, as well as five other cells recorded over the course of these experiments. We measured intrinsic membrane and firing parameters obtained from responses to hyperpolarizing and depolarizing current pulses (Table 1; see METHODS). Intrinsic properties were compared using unpaired Student's *t*-test with the significance level corrected for multiple comparisons. The average age of the animals from which these data were obtained were similar (GAD-GFP: 17.3 ± 2.72 days; wild-type: 17.2 ± 3.2 days) as was the fraction of cells obtained from primary slices (GAD-GFP: 5/13; wild-type: 59/130). We found no differences in intrinsic properties between these two populations (Table 1), indicating that cells from transgenic animals are not adversely affected by expression of GFP.

Distinguishing monofrom polysynaptic responses

We recorded from 73 interneurons in layers I-V of ACx and 41 pyramidal cells in layers II-V. Cells were filled with biocytin and examined after the experiment to confirm their

identification. The morphological properties of the recorded interneurons will be discussed in detail below. Spiny stellate cells were not observed in layer IV, consistent with previous reports in auditory cortex that indicate pyramidal cells are the primary thalamorecipient cells in layer IV (Rose and Metherate 2005; Smith and Populin 2001), but we did not search systematically for cells with spiny stellate morphology in layer IV.

Electrical stimulation of thalamic afferents elicited synaptic responses in 60 interneurons with response latencies varying widely, from 1.45 to 12.9 ms (Fig. 1*A*). In pyramidal cells, responses were elicited in 39 cells, in which latencies ranged from 2.00 to 7.44 ms (Fig. 1*B*). We assume that the shortest response latencies represent monosynaptic connections, whereas the longest latencies, especially in interneurons, may correspond to polysynaptic responses, possibly due to thalamic activation of cortical pyramidal cells that project locally to interneurons. It is very unlikely that the responses recorded here are the result of intracortical projections of pyramidal cells that project to the thalamus and were antidromically activated by the thalamic stimulus, as we never observed antidromic spikes in pyramidal cells during these recordings.

We took three different approaches to distinguish between mono- and polysynaptic responses: comparison of response latencies in interneurons with latencies of thalamically evoked spikes in pyramidal cells, blockade of polysynaptic responses with elevated concentrations of divalent cations in the bath, and analysis of the trial-by-trial variability in response latency in interneurons.

SPIKE LATENCIES IN PYRAMIDAL CELLS—If synaptic responses recorded in interneurons were polysynaptic, these responses would be mediated by thalamic excitation triggering spikes in pyramidal cells that in turn project intracortically to the recorded interneurons. We estimated the minimum latency of such polysynaptic responses in interneurons by measuring the latencies of spikes evoked in pyramidal cells in response to thalamic stimulation (Fig. 2*Ai*). In 10 pyramidal neurons, thalamic stimulation consistently evoked synaptic responses that were large enough to trigger spikes. Mean maximal subthreshold EPSP amplitude in these cells was 15.8 ± 4.1 mV and EPSP latencies averaged 4.39 ± 1.49 ms. Spikes evoked by these EPSPs had latencies that averaged 8.42 ± 2.59 ms (range: 4.3-13.4 ms; Fig. 2*A*, *ii* and *iii*, dashed line), and for most cells, the variability of these spike latencies was small, (mean coefficient of variation = 0.12, range: 0.05-0.29). The shortest latencies of polysynaptic responses in interneurons would then equal these spike latencies plus synaptic and propagation delays, i.e., an average of >9 ms (Fig. 2*Aiii*, thick solid line). There is little overlap between the distribution of these estimated disynaptic excitation latencies and the recorded synaptic latencies in interneurons (Fig. 2 *Aiii*, compare solid thin line with solid thick line), supporting the interpretation that nearly all synaptic responses observed in interneurons are monosynaptic. However, the width of the spike latency distribution observed in pyramidal cells suggest that there may not be a single fixed latency boundary between mono- and polysynaptic responses across all cells and all slices.

One caveat to interpreting these data is that in a given cell, the spike latency would likely be influenced by the cell's resting potential, which is perturbed in whole cell recordings. Thus if a cell is artificially depolarized by perfusion with the pipette solution, spike latency would be expected to be shorter than under physiological conditions, and the opposite effect would be expected if the resting potential was artificially hyperpolarized. However, when we compared responses across cells exhibiting thalamically evoked spikes, we found no correlation between spike latency and resting potential ($r = 0.68$, $P > 0.1$) nor between the resting potential and the lag from EPSP to spike onset ($r = 0.61$, $P > 0.1$), suggesting that spike latency data in these cells was not distorted by artificial changes in resting membrane potential secondary to the recording conditions.

EFFECTS OF HIGH DIVALENT CATIONS—Elevated concentrations of divalent cations have been used to distinguish between mono- and polysynaptic connections in brain slices by raising spike thresholds at each synaptic stage (Berry and Pentreath 1976). When slices are bathed in a solution containing elevated divalent cations, polysynaptic responses should be blocked, whereas monosynaptic responses should be unaffected. We recorded thalamically evoked synaptic responses in eight interneurons in normal ACSF ([Ca] = 2.1 mM, [Mg] = 1.4 mM) and in ACSF with elevated divalent cation concentrations ([Ca] = 4 mM, [Mg] = 4 mM; Fig. 2*B*). In these experiments, synaptic response latencies under control conditions averaged 6.25 ms (range: 4.04-8.07 ms). In the elevated divalent cation solution, the amplitudes of the synaptic responses were largely unaffected (change in amplitude relative to control =-10 ± 20%, $P > 0.3$; Fig. 2*B*), suggesting that in these recordings responses were not polysynaptic. Consistent with polysynaptic responses being suppressed by this treatment, the durations of synaptic responses in interneurons treated with high divalent cations were consistently and reversibly shorter in the presence of high divalent cations (Fig. 2*Bii*), presumably due to longlatency polysynaptic components prolonging the decay of thalamically evoked EPSPs (change in $t_{63\%}$ relative to control = -15 ± 8%, $P < 0.01$). In addition, we recorded responses in pyramidal cells to stimulation of cortical afferents in the white matter, which elicited a monosynaptic EPSP and (presumably) disynaptic IPSP. In bath solution containing elevated divalent cations, the later IPSP was blocked, whereas the early EPSP was preserved (Fig. 2*Biii*). These data suggest that synaptic responses with latencies at least as long as 8 ms are likely to be monosynaptic in these experiments.

VARIABILITY OF SYNAPTIC RESPONSE LATENCY—Finally, polysynaptic responses are reported to have significantly more variable latencies compared with monosynaptic responses (Berry and Pentreath 1976). We quantified the variability of the latency to the onset of the synaptic response to stimulation of thalamic afferents by computing the coefficient of variation of response latency ($Lat_{CV} = Lat_{SD}/Lat_{Mn}$). In interneurons, Lat_{CV} values ranged from 0.02 to 0.21 (Fig. 2*C*). If the longest latency responses were polysynaptic, then we would expect those responses to be the most variable as well, but when Lat_{CV} was plotted as a function of Lat_{Mn}, we observed no such positive correlation (Fig. 2*Cii*). What is apparent from the plot of Fig. 2*Cii* is that the data tend to cluster in the lower left with data from five cells scattered at high Lat_{CV}, high Lat_{Mn}, or both. We chose an arbitrary boundary based on both Lat_{CV} and Lat_{Mn} that was consistent with the experiments on spike latencies in pyramidal cells and experiments with elevated divalent cations. We consider those cells with Lat_{CV} <0.15 and Lat_{Mn} <9.2 ms to be monosynaptically excited by thalamic stimulation, i.e., putative feedforward interneurons (box, Fig. 2*Cii*).

We will give a brief description of the synaptic responses in interneurons and pyramidal cells, and then we will analyze these responses in detail by comparing between cell types, slice of origin, and layer of origin.

Responses to thalamic stimulation in interneurons and pyramidal cells

By the criteria derived in the preceding text, 55 of 60 interneurons were monosynaptically excited by thalamic stimulation, with 26 in primary slices (6 in LI, 10 in LII/III, 7 in LIV, 3 in LV) and 29 in shell slices (2 in LI, 13 in LII/III, 13 in LIV, 1 in LV). These 55 cells are of an original sample of 73 cells, 13 of which exhibited no response to thalamic stimulation and 5 of which exhibited what appeared to be a polysynaptic response. This observation indicates that feedfor-ward inhibition is widespread in ACx with ≥75% of the interneurons in the population recorded directly activated by thalamic stimulation; the number could be higher because the absence of a response could indicate that thalamic afferents to that cell were severed during the slicing procedure.

The early excitatory synaptic responses recorded in all 39 pyramidal cells were monosynaptic by the criteria developed in the preceding text. Twenty three of these cells were located in primary slices (2 in LII/III, 11 in LIV, and 10 in LV), and 16 in shell slices (3 in LII/III, 5 in LIV, and 8 in LV).

Synaptic responses to TC stimulation were usually dominated by excitatory components. We routinely tested for the presence of inhibition by stimulating TC afferents while varying V_m around the Cl^- reversal potential (E_{Cl}; calculated E_{Cl} was -68.5 mV; Fig. 3). To quantify this assessment, we considered the time integral of the normalized evoked synaptic potential (J_{PSP}) as a function of V_m (Fig. 3, *B, D*, and *F*). The function $J_{PSP}(V_m)$ will have nonzero slope only if the kinetics of the underlying PSP vary with voltage. We assume that the AMPA-mediated EPSP has voltage-independent kinetics over the voltage range tested. A disynaptic inhibitory component would contribute negative slope to $J_{PSP}(V_m)$, while activation of an *N*-methyl-D-aspartate (NMDA) component at depolarized potentials will contribute positive slope.

In pyramidal cells, $J_{PSP}(V_m)$ exhibited two dramatically different shapes depending on whether an inhibitory component could be observed in the raw data at depolarized V_m (Fig. 3, *A-D*). In layer V, an inhibitory component was observed in 12 of 18 cells (Fig. 3*A*), and in these 12 cells, $J_{PSP}(V_m)$ dropped precipitously at and positive to E_{Cl} (Fig. 3*B*). By contrast, in pyramidal cells located in layers II-IV ($n = 21$), an inhibitory component was not observed (Fig. 3*C*), and $J_{PSP}(V_m)$ exhibited either zero or positive slope (Fig. 3*D*), the latter suggesting the presence of an NMDA component at depolarized potentials. In all interneurons tested, $J_{PSP}(V_m)$ had zero or positive slope (Fig. 3, *E* and *F*), similar to that observed in layer II-IV pyramidal cells (Fig. 3, *C* and *D*), and in stark contrast to those layer V pyramidal cells exhibiting disynaptic inhibition (Fig. 3, *A* and *B*), indicating that disynaptic inhibition in these cells was absent or extremely weak or less likely that it was exactly balanced by an equal and opposite NMDA component.

We characterized the properties of thalamically evoked EP-SPs in those cells not exhibiting evidence of inhibition (i.e., 55 interneurons and 27 pyramidal cells). In each cell studied, we tested a range of stimulation intensities to determine the maximal response amplitude (Fig. 1). Maximal excitatory synaptic responses in interneurons had mean latencies of ~5 ms, mean EPSP amplitudes of ~5 mV, and durations (t_{HW})of ~26 ms (Table 2). In pyramidal cells, EPSPs had maximal amplitudes of ~11 mV, latencies of ~4 ms, and half-widths of ~35 ms (Table 2). Next we will analyze the response properties of interneurons and pyramidal cells in more detail by comparing synaptic responses and intrinsic properties according to cell type and slice of origin.

Cell-type specificity of thalamic synaptic responses in ACx

We first compared the amplitude, latency and duration of maximal EPSPs evoked by thalamic stimulation in all GFP-positive interneurons with those elicited in all pyramidal cells that did not exhibit disynaptic inhibition, using unpaired Student's *t*-test (Table 2). To correct for multiple (i.e., 3) comparisons, we used a significance level of $P < 0.0167$. Significant differences were observed in all three synaptic parameters (Table 2).

Thalamic responses in the layer V pyramidal cells exhibiting inhibition were always subthreshold. In contrast, TC responses in pyramidal cells not exhibiting inhibition were superthresh-old in 11 of 27 cells (Fig. 1*B*), though spiking was far more common in primary slices (9 of 17 cells) than in shell slices (2 of 10 cells). In contrast to pyramidal cells, thalamic responses in interneurons were rarely superthreshold (3 of 55 cells; Fig. 1*A*). Because spike thresholds in response to depolarizing current pulses were not different between the two cell populations (pyramidal cells: 28.4 ± 5.94 mV; interneurons: 27.8 ± 5.78 mV; $P > 0.6$, Student's

t-test), this difference in the effectiveness of thalamic excitation is likely exclusively due to the smaller EPSP amplitudes observed in interneurons compared with pyramidal cells (Table 2).

It is reasonable to expect that the cells in primary versus shell slices would differ in the strength and latency of excitation evoked in auditory cortex based on proposed differences in coding properties of cells in primary versus nonprimary thalamus and cortex (Hu 2003;Jones 1998) and on differences in anatomical properties of TC projections (Cetas et al. 1999). By comparing the properties of cells in primary versus shell slices, we are able to evaluate these predictions at the single-cell level. Interneurons in primary slices were divided into two groups: those located in layers III (i.e., the deep half of layer II/III), IV, and V were considered to be most heavily representative of cells along the lemniscal pathway, whereas those located in layers I and II (i.e., in the superficial half of layer II/III) were grouped separately as they could be activated either by fibers of the lemniscal or extralemniscal pathway. It should be noted that this division is only approximate because the division between primary and secondary auditory cortex was unlikely to occur exactly at the boundary between the primary and shell slices. In addition, interneurons in layer IV in primary auditory cortex could still have some dendritic processes extending into layer I (see Fig. 7, cell 4). Interneurons in shell slices were divided similarly into two groups, LI-II and LIII-V cells. Both of these groups were considered to be composed mostly of cells in the extralemnsical pathway, again subject to the caveat that the boundary between primary and secondary ACx was unlikely to coincide exactly with the boundary between primary and shell slices. One-way ANOVA was used to compare the amplitude, duration and latency of maximal (subthreshold) synaptic responses (Table 2) and intrinsic membrane and firing properties (Table 3) across the six categories of cell type (primary LI-II interneuron, primary LIII-V interneuron, shell LI-II interneuron, shell LIII-V neuron, primary pyramidal cell, and shell pyramidal cell). Synaptic response parameters are described first (Fig. 4; Table 2), whereas intrinsic properties are described in the next section (Fig. 5; Table 3).

Significant effects of cell type were found for A_{EPSP}. Lat_{Mn}, and $t_{HW,\ EPSP}$ (Fig. 4; Table 2). Post hoc tests indicated that there were no significant differences between primary and shell pyramidal cells for any of the synaptic response parameters. EPSP amplitudes were smaller in all classes of interneurons compared with primary pyramidal cells, whereas EPSP latencies were longer in both classes of shell interneurons compared with primary pyramidal cells. EPSP durations were shorter in primary LI-II interneurons compared with primary and shell pyramidal cells as well as primary LIII-V interneurons (Fig. 4; Table 2). Thus the difference in EPSP latency observed between interneurons and pyramidal cells is driven largely by shell interneurons, whereas differences in amplitude are distributed across multiple cell types and differences in duration are driven largely by superficial primary interneurons. In general, however, we detected few differences between cells in primary versus shell slices. Latencies and amplitudes in primary versus shell pyramidal cells were statistically indistinguishable, and although latencies in shell interneurons were the longest of any cell type, these latencies were not statistically different from those observed in interneurons from primary slices.

We also considered how the properties of synaptic responses varied as a continuous function of depth relative to the cortical surface [$d_{frac} \in (0,1)$; Fig. 4]. There was no significant correlation between d_{frac} and EPSP amplitude or duration for interneurons or pyramidal cells from either primary or shell slices (Fig. 4, *A* and *C*). For interneurons in primary slices, excluding one outlier cell in deep layer V, latency tended to decrease with cortical depth; this was not true for interneurons from shell slices (Fig. 4*B*). This is consistent with previous reports indicating that latencies in layer IV of primary slices are the shortest observed in ACx in response to TC stimulation (Cruikshank et al. 2002). Interestingly, the same correlation with depth was observed for pyramidal cells in primary slices (with nearly identical slope and

intercept, again excluding one outlier cell in deep LV) but not for pyramidal cells in shell slices (Fig. 4*B*). The latencies of EPSPs was longer on average in interneurons compared with pyramidal cells, a result that contrasts with previous reports in somatosensory cortex (Agmon and Connors 1992). However, when the comparison is made between only cells located in layer IV of primary slices, Lat_{Mn} was comparable (interneurons: 4.08 ± 1.44 ms, $n = 7$; pyramidal cells 3.88 ± 1.41, $n = 13$; Fig. 4*B*), similar to previous observations in primary auditory TC slices (Rose and Metherate 2005).

As illustrated in Fig. 4*A*, there was no evidence for spatial clustering of cells with large amplitude synaptic responses, suggesting that we did not encounter a subtype of interneuron strongly excited by TC afferents among our sample. For example, fast spiking (FS) cells of layers IV and V are reported to exhibit the strongest thalamic excitation among cells in somatosensory cortex (Gibson et al. 1999). We encountered six cells in layer IV (3 primary, 3 shell) the firing properties of which are similar to those of FS cells, i.e., $ISI_{Ratio} > 0.8$, where the ISI_{Ratio} is calculated from the response to a depolarizing current pulse and equals the first interspike interval during the response divided by the last (Porter et al. 2001). In these six cells, $Lat_{Mn} = 3.95 \pm 1.78$ ms, $Lat_{CV} = 0.0659 \pm 0.0312$, and $t_{HW} = 35.6 \pm 24.9$ ms. None of these cells fired action potentials in response to thalamic stimulation, and the mean EPSP amplitude for these cells was 5.59 mV (range: 1.74-13.5 mV), similar to the population average (5.26 mV).

Cell-type specificity of intrinsic properties

The synaptic properties presented in the preceding text represent largely passive responses to excitatory inputs from the thalamus, but differences in these properties could be influenced by differences in membrane properties across cell type. In addition, the superthreshold response to thalamic inputs and any coincident intracortical or sub cortical inputs will be influenced by the cells' firing properties. We used responses to depolarizing and hyperpolarizing current pulses to characterize the passive properties and firing behavior of the recorded cells (Fig. 5; Table 3). We intended to use these measurements to develop a quantitative and objective classification scheme to be applied in particular to interneurons. However, the intrinsic parameters of interneurons were heterogeneous (Figs. 6 and 7) and appeared to represent continua rather than discreet groups (not shown; see METHODS). Similarly, responses in pyramidal cells could be classified qualitatively as regular spiking or intrinsic bursting, but the distinction between these two firing types was not as clear as in ACx of the rat (Hefti and Smith 2000), and we did not attempt to classify these cell types quantitatively. Instead, we compared the intrinsic properties across the six cell types the synaptic response properties of which were described in the preceding text.

Subthreshold properties were characterized by the estimated membrane time constant (τ_{mem}), estimated resting input resistance (R_{IN}) and ratio of the peak to steady-state *I-V* slope ($I\text{-}V_{Slope\ ratio}$), the latter a measure of the magnitude of I_h in these cells. Excitability was parameterized by spike threshold (V_{Thresh}) and the slope of the current-spike frequency relationship ($I\text{-}f_{Slope}$), adaptation by the ratio of the first to last interspike intervals during a 250-ms, 25-Hz spike train (ISI_{Ratio}), spike shape by spike amplitude (A_{Spk}) and duration ($t_{HW,\ spk}$), and AHP shape by its amplitude (A_{AHP}) and normalized time of peak ($t_{pk,\ AHP}$).

There were few differences in intrinsic properties among the four groups of interneurons. One difference that was observed may underlie the shorter EPSP durations observed in LI-II interneurons in primary slices: these cells had the shortest estimated τ_{mem} of the six cell classes, and this difference was significant relative to shell LIII-V interneurons and both types of pyramidal cells (Fig. 5*A*; Table 3). Several other parameters differed significantly between pyramidal cells and multiple classes of interneurons. Input resistance was significantly larger in all classes of interneurons compared with both classes of pyramidal cells (Fig. 5*B*; Table 3).

Similarly, $I\text{-}f_{Slope}$ was larger in interneurons than in pyramidal cells, and this difference was significant for both types of primary interneurons and shell LIII-V cells compared with primary and shell pyramidal cells (Fig. 5*C*, Table 3). Spike amplitude was smaller in interneurons compared with pyramidal cells with significant differences observed between pyramidal cells and both types of shell interneurons and primary LI-II cells (Fig. 5*D*; Table 3). The shape of the AHP was also different between interneurons and pyramidal cells, with $t_{AHP,\ pk}$ significantly smaller (i.e., the AHP peaks earlier in the interspike interval) in both types of primary interneurons and shell LIII-V interneurons compared with primary and shell pyramidal cells (Fig. 5*E*; Table 3). We did not observe any significant differences in intrinsic properties between primary and shell pyramidal cells (Table 3). Two parameters increased systematically with cortical depth: τ_{mem} in primary interneurons (Fig. 5*A*), and A_{Spk} in shell interneurons (Fig. 5*D*). These results suggest that the intrinsic properties of interneurons in ACx were similar across the four cell types we considered but were largely distinct from intrinsic properties of pyramidal neurons.

Analysis of developmental changes in synaptic and intrinsic properties

Synaptic connections in the auditory thalamocortical slice preparation are most intact in slices obtained from animals ~2-3 wk old. Because changes in the intrinsic properties of neurons during this age have been reported previously (Christophe et al. 2005; Connors 1994), we investigated whether any of the synaptic or intrinsic properties we measured here were affected by the age of the animal from which slices were obtained. To determine which parameters changed over the age range used here (P13-P25), we used multivariate regression with animal age as the independent variable and synaptic and intrinsic response properties (Lat_{Mn}, A_{EPSP}, $t_{HW,\ EPSP}$, τ_{mem}, R_{IN}, $I\text{-}V_{Slope\ ratio}$, V_{Thresh}, $I\text{-}f_{Slope}$, ISI_{Ratio}, A_{Spk}, $t_{HW,\ spk}$, A_{AHP}, and $t_{pk,\ AHP}$) as dependent variables. We ran the model first on all of the data grouped across cell types. Model parameters were the slope coefficient (B) for each independent variable and the significance of its difference from zero. None of the synaptic response parameters depended significantly on animal age (Lat_{Mn}:B =-0.034, $P = 0.577$; A_{EPSP}:B =-0.058, $P = 0.733$; $t_{HW,\ EPSP}$:B =-0.525, $P = 0.321$). Of the parameters describing intrinsic properties, two changed significantly with age: τ_{mem} (B =-0.823, $P = 0.001$) decreased from 21.4 ± 7.54 ms at P13-14 ($n = 20$) to 12.8 ± 3.72 ms at P22-25 ($n = 17$), and V_{Thresh} (B =-0.460, $P = 0.01$) decreased from -34.8 ± 4.65 mV at P13-14 to -40.6 ± 4.95 mV at P22-25.

Having observed that some parameters varied significantly with age, we checked whether the effect of age could explain the differences in intrinsic and synaptic properties observed across cell type and described in the preceding text. The multivariate regression model was expanded to include both animal age and cell type (i.e., LI-II primary and shell interneurons, LIII-V primary and shell interneurons, and primary and shell pyramidal cells) as independent variables. A third dependent variable, the interaction term [animal age]*[cell type], was included in the model to capture any differential effects of age that depended on cell classification. None of the coefficients for this interaction term were significantly different from zero for any of the independent variables (not shown), indicating that the effects of age on measured parameters were indistinguishable across cell type, and thus the differences between cell type observed for synaptic and intrinsic properties were not due to the effects of animal age.

Morphology of interneurons

Recorded interneurons were labeled with biocytin and two-dimensional projections of their axonal and dendritic fields were drawn using camera lucida. Twenty interneurons were labeled well enough to determine detailed dendritic morphology and axonal projection patterns, and nine of these cells are illustrated in Figs. 6 (primary slices) and 7 (shell slices). To quantify the extent and orientation of a cell's axonal field, we drew rectangles encompassing the two-

dimensional projection of the terminal field in our camera lucida drawings and measured the vertical (i.e., mediolateral) and horizontal (i.e., rostrocaudal) dimensions of the rectangle, and their ratio (as a measure of orientation). In addition, we estimated the density of axonal swellings labeled for each cell (see METHODS).

Putative feedforward interneurons in our sample were located throughout layers I-V in both shell and primary slices. In layer I, cells were typically oriented horizontally, with dendrites and axon usually confined to layer I (Figs. 6 and 7). In four labeled cells analyzed in detail, the horizontal (i.e., withinlayer) extent of the axonal projection was ~750 μm (range: 690-817 μm) and the orientation ratio was ~3.5 (range: 2.0-4.6). The estimated density of putative boutons was ~23/100 μm^3 (i.e., a count of ~1,800 putative boutons in these slices; range: 15-28/100 μm^3). Thus layer I cells were poised to contact large numbers of pyramidal cells and interneurons in layer I over a wide horizontal extent of cortex.

The dendritic morphology of interneurons in layers II/III was typically multipolar. Axonal fields were extensive, with the horizontal extent ~550 μm (range: 240-894 μm; $n = 9$ cells), vertical extent ~615 μm (range: 280-1,011 μm), and the orientation ratio ~0.96 (range: 0.39-1.36). Axonal projections were typically densest within layer II/III, but strong projections were observed in layer IV and projections could reach layers I and V as well (Figs. 6 and 7). The estimated density of putative boutons was ~33/100 μm^3 (i.e., a count of ~3,200 putative boutons in these slices; range: 5-137/100 μm^3).

Interneurons in layer IV had either multipolar or vertically oriented (i.e., perpendicular to the cortical laminae) bipolar dendritic morphology (Figs. 6 and 7). Axonal fields were more vertically oriented than those in the more superficial layers with horizontal extent ~430 μm (range: 128-640 μm; $n = 5$ cells), vertical extent ~505 μm (range: 242-1,037 μm), and orientation ratio ~0.88 (range: 0.53-1.25). Although projections still tended to be densest within layer IV, the distribution of boutons was more uniform across layers than for layer II/III cells, and extensive projections into layers V and II/III were observed (Figs. 6 and 7). The estimated density of putative boutons was ~22/100 μm^3 (i.e., a count of ~2,480 putative boutons in these slices; range: 6-47/100 μm^3).

In comparing labeled cells in primary versus shell slices, there were no significant differences in the extent or orientation of the axonal arbor or in the estimated density of putative synaptic boutons (not shown). Thus cells throughout layers I-V in both primary and shell slices are poised to have widespread influence on the activity of other cortical cells, through convergence of many inputs onto individual target cells, divergence onto many target cells, or both.

DISCUSSION

Summary

We studied the synaptic responses of interneurons in ACx of GAD65-eGFP transgenic mice and compared these responses to those of pyramidal cells. For this population of interneurons, we found evidence that thalamic afferents directly excited >75% of cells in layers I-V. These cells had widespread and dense axonal termination patterns in ACx. However, the function of this thalamic excitation is unclear, as maximal EPSP amplitudes were small and subthreshold in 95% of cells tested. In comparison, thalamic EPSPs in pyramidal cells located in layers II-V that did not exhibit disynaptic inhibition were significantly larger than in interneurons and were superthreshold in >40% of cells. We conclude that thalamic excitation of interneurons in ACx is widespread, but in many cases, targeted cells would require coincident excitation from within neocortex or from subcortical neuromodulators to be activated by thalamic inputs.

Feedforward inhibition in sensory neocortex

Thalamic afferents contact several classes of interneurons in somatosensory and auditory cortex. Some of these cells form homogeneous groups and exhibit similar response properties to thalamic stimulation. For example, FS cells in layers IV and V are strongly activated by thalamic inputs in somatosensory cortex, whereas low-threshold spiking (LTS) cells in this region are weakly excited (Gibson et al. 1999). However, there are numerous classes of neocortical interneurons (Markram et al. 2004), and it is clear that thalamic afferents contact many of these classes (Porter et al. 2001). Although the fibers from primary thalamus (i.e., ventral medial geniculate) terminate most densely in deep layer III and layer IV, these fibers can also target layer I (Cetas et al. 1999). In addition, fibers originating in areas of medial geniculate outside of the ventral division target all layers diffusely in nonprimary ACx and terminate densely in layer I in primary ACx (Kimura et al. 2003; Linke and Schwegler 2000; Lorente De No 1938). We show here that that there are interneurons throughout layers I-V in ACx that are directly excited by thalamic afferents that likely originate from both primary and nonprimary thalamus. However, the strength of this excitation is weak, requiring coincident inputs from other cortical regions (Vogt 1991) or activation of these interneurons by neuromodulators (Kawaguchi 1997) to be effective.

It is unclear whether the cells in our sample represent a subpopulation of weakly excited interneurons that may only be recruited into feedforward inhibitory circuits during periods of enhanced intracortical or subcortical activation or whether feedforward inhibition in ACx is organized differently from other sensory cortices and that only a minority of interneurons that target layer V cells are strongly excited by thalamic afferents. The former possibility suggests that future recordings targeted to layer IV of primary ACx will identify strongly excited interneurons similar to those described in somatosensory cortex. Interestingly, the latter possibility is consistent with our observations on feedforward inhibition in pyramidal cells and our recordings from a small sample of FS-like cells as well. One previous study in layer IV of ACx showed that FS cells are contacted by thalamic afferents (Rose and Metherate 2005), but these cells were studied only with minimal stimulation, and thus it is unclear whether thalamic inputs were superthreshold. These responses were similar to those reported here in that the duration of EPSPs in the FS-like cells we recorded (35.6 ms) was comparable to that reported by Rose and Metherate (2005), but Lat_{Mn} was substantially less (3.95 ms in our data vs. 7.38 ms) possibly due to differences in the location of the stimulation electrode.

Interneurons in GAD65-eGFP mice

The population of interneurons studied here is the subject of a recent report on the properties of a subpopulation of cells expressing the cannabanoid receptor CB_1 (Galarreta et al. 2004). In this study, the only one to date to probe the electrophysiological properties of interneurons in these transgenic animals, the authors focused on the properties of large, irregularly spiking interneurons in layer II/III of somatosensory cortex that selectively express CB_1 and are preferentially connected to each other via gap junctions. The responses to thalamic stimulation were not studied. Although we did not test for the expression of CB_1, we encountered several large interneurons in layer II/III (Figs. 6 and 7) that responded to thalamic stimulation, but the responses of these cells to depolarizing current injection were heterogeneous with some cells exhibiting slightly irregular firing patterns due to "missed" spikes during a regular, periodic response (Fig. 6, green cell), whereas others exhibited adapting but regular spiking patterns (Figs. 6, red cell, and 7, *green cell)*. Our data indicate that large interneurons in layer II/III of these transgenic animals may be more heterogeneous than previously reported.

This heterogeneity was a general feature of the intrinsic properties of interneurons expressing GAD 65-eGFP (Figs. 5-7). However, when considered in terms of the four broad categories of interneurons we defined, there were few parameters that varied systematically between

interneuronal cell types, indicating that response properties were equally heterogeneous in these four types. In contrast, interneurons and pyramidal cells differed systematically in their intrinsic properties (Fig. 5; Table 3).

Weak feedforward inhibition in supragranular layers

One of our most striking findings is the relative weakness of feedforward inhibition in layers II-IV of the auditory TC slice preparation. We observed no disynaptic inhibition in pyramidal cells in these layers on stimulation of TC afferents, and the strength of excitation in the population of interneurons recorded here was roughly half that observed in pyramidal cells (Table 2) and rarely elicited action potentials. This is in contrast to the somatosensory TC slice preparation in which thalamic excitation of excitatory cells in layers II/III is weak, and disynaptic inhibition is often observed in these cells even in the absence of monosynaptic excitation (Agmon and Connors 1992).

Previous studies of feedforward inhibition in sensory cortex have focused almost exclusively on the responses to thalamic stimulation of cells located in layer IV, classically defined as the thalamorecipient layer in sensory cortex. Not surprisingly, interneurons in layer IV exhibit large-amplitude, often superthreshold responses to TC stimulation and likely contribute to fast and strong feedforward inhibition during sensory stimulation. We chose instead to investigate the properties of a population of interneurons spanning layers I-V and found a very different response profile. In these cells, thalamic excitation was common, occurring in >75% of cells tested, but was weak, both relative to excitation in pyramidal cells and relative to spike threshold. Even EPSPs evoked in layer IV interneurons exhibiting little adaptation, similar to FS cells, were small compared with those evoked in pyramidal cells, and none of these cells fired action potentials in response to TC stimulation. Indeed, the responses of cells in primary slices, which contain a dense thalamic projection from the ventral division of the medial geniculate to layer IV, were statistically indistinguishable from those in shell slices, in which thalamic projections are more diffuse (Table 2; Fig. 4). We observed no dependence of response amplitude on the cortical depth of the cell in either shell or primary slices, indicating for example that layer IV cells in primary slices, where we would expect the heaviest innervation by TC afferents, were no more likely to receive strong TC excitation than cells in more superficial layers. We speculate that the inhibitory cells studied here would only play a role in feedforward inhibition when the context of the stimulus or behavioral state of the animal triggered additional, coincident excitation to these interneurons. This may represent an organizing principal of feedforward inhibition in neocortex, with strongly excited (e.g., FS) cells active under normal or quiescent conditions, and additional inhibitory cells recruited under more specialized conditions.

ACKNOWLEDGMENTS

The authors thank R. Burlingame, C. Cotter, N. Rogge, M. Rummel, and A. Schuh for technical support and P. H. Smith for comments on the manuscript.

REFERENCES

Agmon A, Connors BW. Correlation between intrinsic firing patterns and thalamocortical synaptic responses of neurons in mouse barrel cortex. J Neurosci 1992;12:319–329. [PubMed: 1729440]

Banks MI, Pearce RA, Smith PH. Hyperpolarization-activated cation current (I_H) in neurons of the medial nucleus of the trapezoid body-voltageclamp analysis and enhancement by norepinephrine and camp suggest a modulatory mechanism in the auditory brain stem. J Neurophysiol 1993;70:1420–1432. [PubMed: 7506755]

Berry MS, Pentreath VW. Criteria for distinguishing between monosynaptic and polysynaptic transmission. Brain Res 1976;105:1–20. [PubMed: 175886]

Cetas JS, de Venecia RK, McMullen NT. Thalamocortical afferents of Lorente de No: medial geniculate axons that project to primary auditory cortex have collateral branches to layer I. Brain Res 1999;830:203–208. [PubMed: 10350577]

Christophe E, Doerflinger N, Lavery DJ, Molnar Z, Charpak S, Audinat E. Two populations of layer V pyramidal cells of the mouse neocortex: development and sensitivity to anesthetics. J Neurophysiol 2005;94:3357–3367. [PubMed: 16000529]

Cipolloni PB, Keller A. Thalamocortical synapses with identified neurons in monkey primary auditory cortex: a combined Golgi/EM and GABA/peptide immunocytochemistry study. Brain Res 1989;492:347–355. [PubMed: 2568876]

Connors BW. Intrinsic neuronal physiology and the functions, dysfunctions and development of neocortex. Prog Brain Res 1994;102:195–203. [PubMed: 7800812]

Connors BW, Gutnick MJ. Intrinsic firing patterns of diverse neocortical neurons. Trends Neurosci 1990;13:99–104. [PubMed: 1691879]

Cruikshank SJ, Rose HJ, Metherate R. Auditory thalamocortical synaptic transmission in vitro. J Neurophysiol 2002;87:361–384. [PubMed: 11784756]

Defelipe J. Types of neurons, synaptic connections and chemical characteristics of cells immunoreactive for calbindin-d28k, parvalbumin and calretinin in the neocortex. J Chem Neuroanat 1997;14:1–19. [PubMed: 9498163]

Foeller E, Vater M, Kossl M. Laminar analysis of inhibition in the gerbil primary auditory cortex. J Assoc Res Otolaryngol 2001;2:279–296. [PubMed: 11669400]

Galarreta M, Erdelyi F, Szabo B, Hestrin S. Electrical coupling among irregular-spiking GABAergic interneurons expressing cannabinoid receptors. J Neurosci 2004;24:9770–9778. [PubMed: 15525762]

Gibson JR, Beierlein M, Connors BW. Two networks of electrically coupled inhibitory neurons in neocortex. Nature 1999;402:75–79. [PubMed: 10573419]

Hefti BJ, Smith PH. Anatomy, physiology, and synaptic responses of rat layer V auditory cortical cells and effects of intracellular GABA(A) blockade. J Neurophysiol 2000;83:2626–2638. [PubMed: 10805663]

Hu B. Functional organization of lemniscal and nonlemniscal auditory thalamus. Exp Brain Res 2003;153:543–549. [PubMed: 12937877]

Jones EG. Viewpoint: the core and matrix of thalamic organization. Neuroscience 1998;85:331–345. [PubMed: 9622234]

Kawaguchi Y. Selective cholinergic modulation of cortical gabaergic cell subtypes. J Neurophysiol 1997;78:1743–1747. [PubMed: 9310461]

Kimura A, Donishi T, Sakoda T, Hazama M, Tamai Y. Auditory thalamic nuclei projections to the temporal cortex in the rat. Neuroscience 2003;117:1003–1016. [PubMed: 12654352]

Linke R, Schwegler H. Convergent and complementary projections of the caudal paralaminar thalamic nuclei to rat temporal and insular cortex. Cereb Cortex 2000;10:753–771. [PubMed: 10920048]

Lopez-Bendito G, Sturgess K, Erdelyi F, Szabo G, Molnar Z, Paulsen O. Preferential origin and layer destination of GAD65-GFP cortical interneurons. Cereb Cortex 2004;14:1122–1133. [PubMed: 15115742]

Lorente De No, R. Cerebral cortex: Architecture, intra-cortical connextions, motor projections. In: Fulton, J., editor. Physiology of the Nervous System. Oxford Univ. Press; Oxford, UK: 1938. p. 291-340.

Lorente De No R. The cerebral cortex of the mouse (a first contribution-the "acoustic" cortex). Somatosens Mot Res 1992;9:3–36. [PubMed: 1317625]

Markram H, Toledo-Rodriguez M, Wang Y, Gupta A, Silberberg G, Wu CZ. Interneurons of the neocortical inhibitory system. Nat Rev Neurosci 2004;5:793–807. [PubMed: 15378039]

Meyer AH, Katona I, Blatow M, Rozov A, Monyer H. In vivo labeling of parvalbumin-positive interneurons and analysis of electrical coupling in identified neurons. J Neurosci 2002;22:7055–7064. [PubMed: 12177202]

Mitani A, Shimokouchi M, Itoh K, Nomura S, Kudo M, Mizuno N. Morphology and laminar organization of electrophysiologically identified neurons in the primary auditory cortex in the cat. J Comp Neurol 1985;235:430–447. [PubMed: 3998218]

Muller CM, Scheich H. Contribution of GABAergic inhibition to the response characteristics of auditory units in the avian forebrain. J Neuro-physiol 1988;59:1673–1689.

Oliva AA, Jiang MH, Lam T, Smith KL, Swann JW. Novel hippocampal interneuronal subtypes identified using transgenic mice that express green fluorescent protein in GABAergic interneurons. J Neurosci 2000;20:3354–3368. [PubMed: 10777798]

Porter JT, Johnson CK, Agmon A. Diverse types of interneurons generate thalamus-evoked feedforward inhibition in the mouse barrel cortex. J Neurosci 2001;21:2699–2710. [PubMed: 11306623]

Roger M, Arnault P. Anatomical study of the connections of the primary auditory area in the rat. J Comp Neurol 1989;287:339–356. [PubMed: 2778109]

Rose HJ, Metherate R. Auditory thalamocortical transmission is reliable and temporally precise. J Neurophysiol 2005;94:2019–2030. [PubMed: 15928054]

Scheel M. Topographic organization of the auditory thalamocortical system in the albino rat. Anat Embryol 1988;179:181–190. [PubMed: 3232855]

Smith PH, Populin LC. Fundamental differences between the thalamocortical recipient layers of the cat auditory and visual cortices. J Comp Neurol 2001;436:508–519. [PubMed: 11447593]

Staiger JF, Zilles K, Freund TF. Distribution of GABAergic elements postsynaptic to ventroposteromedial thalamic projections in layer IV of rat barrel cortex. Eur J Neurosci 1996;8:2273–2285. [PubMed: 8950092]

Vogt, BA. The role of layer I in cortical function. In: Peters, A.; Jones, EG., editors. Cerebral Cortex. Plenum; New York: 1991. p. 49-79.

Volkov IO, Galazjuk AV. Formation of spike response to sound tones in cat auditory cortex neurons: interaction of excitatory and inhibitory effects. Neuroscience 1991;43:307–321. [PubMed: 1922775]

Wang J, Caspary D, Salvi RJ. $GABA_A$ antagonist causes dramatic expansion of tuning in primary auditory cortex. Neuroreport 2000;11:1137–1140. [PubMed: 10790896]

White EL, Keller A. Intrinsic circuitry involving the local axon collaterals of corticothalamic projection cells in mouse SmI cortex. J Comp Neurol 1987;262:13–26. [PubMed: 3624546]

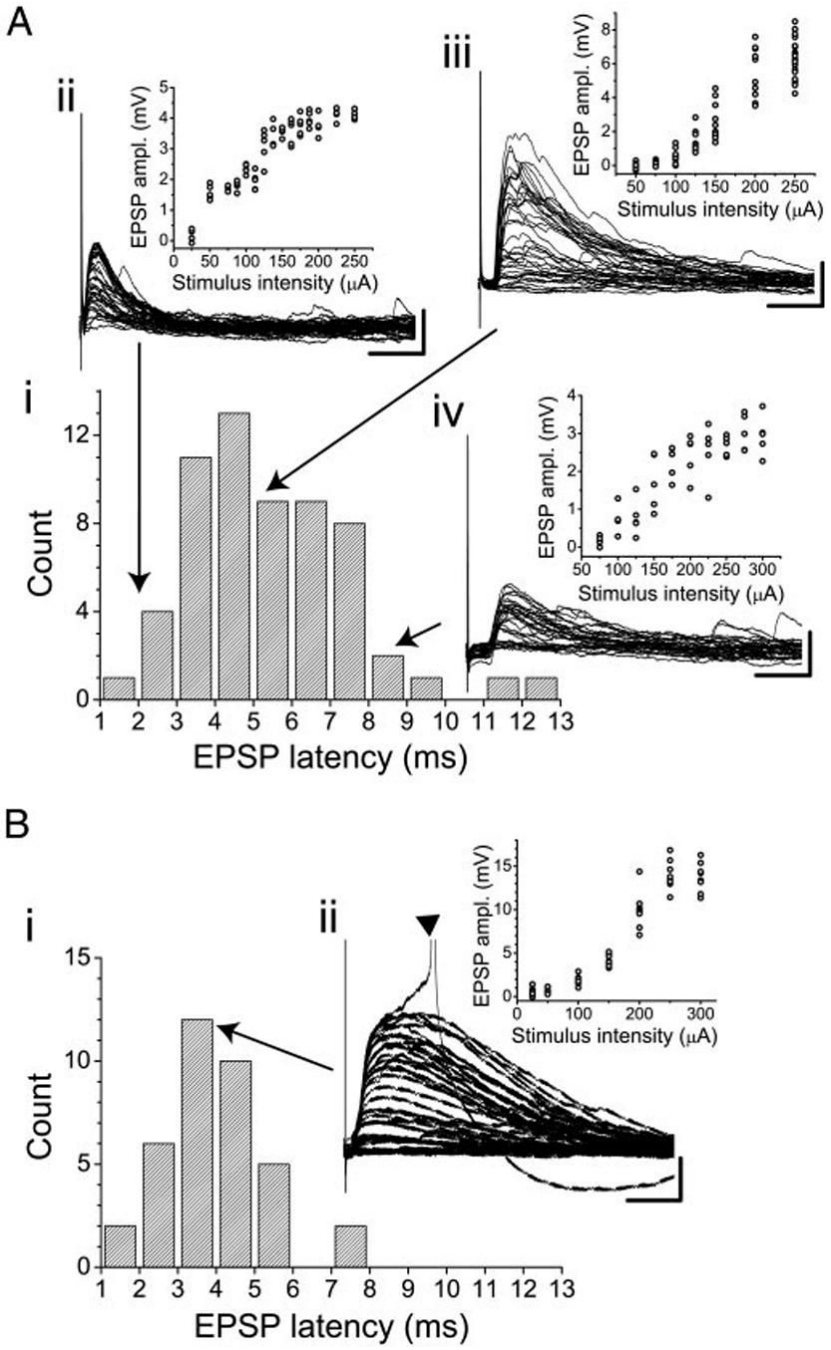

FIG. 1.

Latency distributions (*Ai* and *Bi*) and example current-clamp responses to thalamic stimulation in interneurons (*A*, *ii*-*iv*) and a layer IV pyramidal cell (*Bii*). In *A*, 3 examples are illustrated, representing short (*ii*)-, medium (*iii*)-, and long (*iv*)-latency responses. For each cell, the raw traces and the stimulus-response curve are shown. Resting potentials for the cells illustrated are as follows: *Aii*, -70.7 mV; *Aiii*, -74.7 mV; *Aiv*, -73.4 mV; *Bii*, -71.2 mV. Scale bars: *A*, 20 ms, 2.5 mV; *B*, 20ms, 5mV. ▼ in *Bii* marks a truncated action potential.

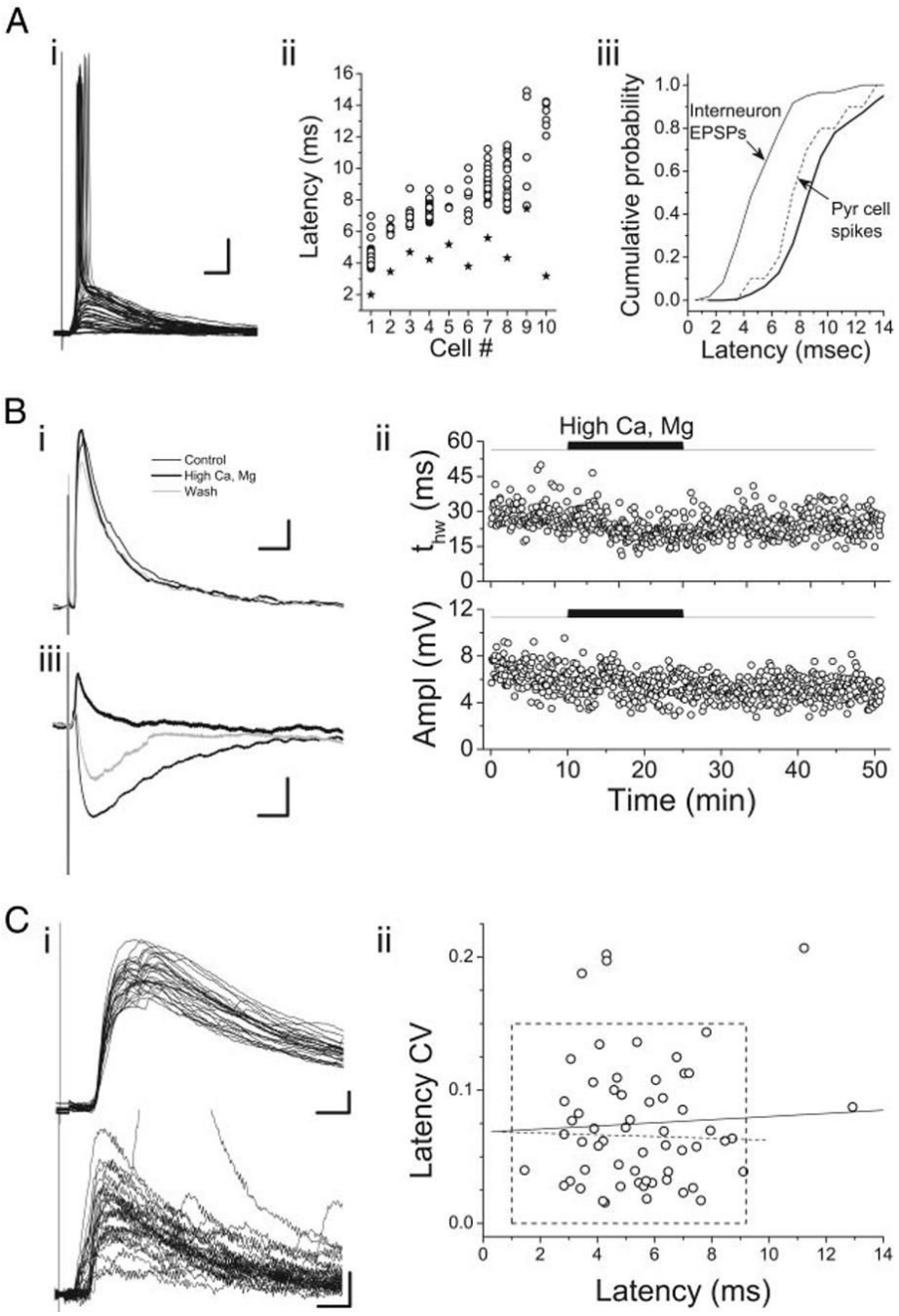

FIG. 2.

Distinguishing monofrom polysynapt1ic synaptic responses to thalamic stimulation. *A*: spike latencies in layer II-IV pyramidal cells. Raw responses of a single pyramidal cell (*i*) and spike latencies for 10 cells (*ii*, open circles) in which thalamic stimulation was superthreshold. Multiple symbols for each cell represent latency measurements in different trials. Also shown in *ii* are mean EPSP latencies for each cell (stars). Cells are ordered along the horizontal axis according to mean spike latency. In *iii*, cumulative latency distributions are shown for excitatory postsynaptic potentials (EPSPs) in interneurons (thin solid line) and spikes in pyramidal cells (thin dashed line). Thick solid line is the distribution of pyramidal cell spike latencies smoothed and shifted 1 ms to the right, representing the estimate of disynaptic EPSP

latencies expected from the pyramidal cell spike latency data. Resting potential for the cell in *i* was -72.6 mV. Scale bars: 10 ms, 10 mV. *B*: effects of elevated extracellular divalent cations on synaptic responses in auditory thalamocortical (TC) slices. *Bi*: average synaptic response to TC stimulation in a layer II interneuron from a primary slice in control (thin black trace), 4 mM [Ca^{2+}] and 4 mM [Mg^{2+}] (thick black trace), and recovery (gray trace). Resting potential, -76.1 mV. *Bii*: time-series plot of EPSP duration (t_{HW}) and amplitude for the same experiment as in *Bi*. *Biii*: average synaptic response to stimulation in the white matter of a layer IV pyramidal cell in control (thin black trace), 4 mM [Ca^{2+}] and 4 mM [Mg^{2+}] (thick black trace), and recovery (gray trace). Cell was held at -50 mV during the stimulation to make the disynaptic inhibitory postsynaptic potential (IPSP) visible. Scale bars: 25 ms, 1 mV. *C*: analysis of the variability of response latency in interneurons. *i*: 2 example responses to TC stimulation, 1 with low Lat_{CV}(*top*; Lat_{CV} = 0.02; E_{Rest} =-66.1 mV; layer II/III interneuron) and 1 with high Lat_{CV} (*bottom*; Lat_{CV} = 0.20; E_{Rest} =-67.6 mV; layer II/III interneuron). *ii:* mean Lat_{CV} as a function of Lat_{Mn} for all 60 interneurons exhibiting responses to thalamic stimulation. Dashed box, boundaries of putative monosynaptic responses, i.e., Lat_{CV}<0.15 and Lat_{Mn} <9.25 ms. Dashed line, linear regression fit to the data within the dashed box. Solid line, linear regression fit to all of the data. Neither line had significant nonzero slope.

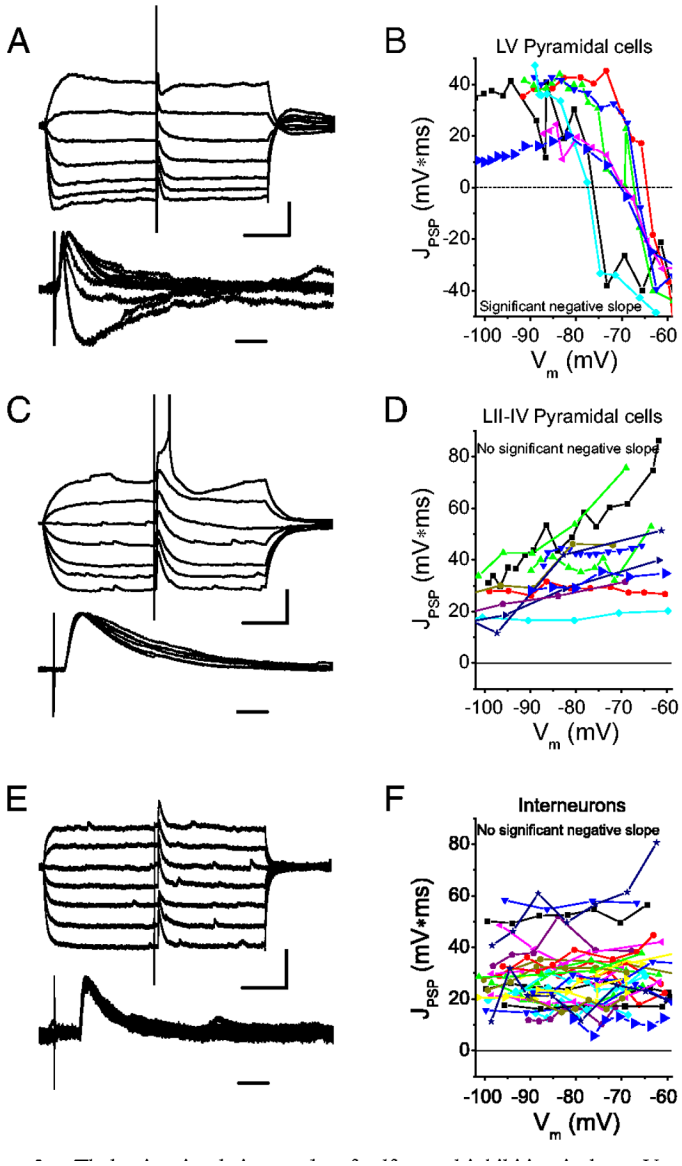

FIG. 3.

Thalamic stimulation evokes feedforward inhibition in layer V pyramidal cells (*A* and *B*) but not in layer II-IV pyramidal cells (*C* and *D*) or in interneurons (*E* and *F*). Cells were hyper- and depolarized about E_{Rest} with 250-ms current steps, and thalamic afferents stimulated at constant intensity (*A*, *C*, and *E*, *top*). Responses were then normalized and aligned (*A*, *C*, and *E*, *bottom*) and the time integral of the response computed (J_{PSP}; *B*, *D*, and *F*, large symbols). This analysis was repeated for all cells in which ≥3 membrane potentials were tested (*B*, *D*, and *F*, small symbols). For pyramidal cells in layer V, inhibition was apparent in the responses and $J_{PSP}(V_m)$ had significant negative slope (*B*). For pyramidal cells in layers II-IV (*D*) and interneurons (*F*), no inhibition was apparent and $J_{PSP}(V_m)$ did not have significant negative slope. Resting potentials were -78.2 mV (*A*), -75.1 (*C*), -67.9 mV (*E*). Scale bars: 100 ms, 10 mV (*A* and *C*, *top*); 100 ms, 6 mV (*E*, *top*); 10 ms (*A*, *C*, and *E*, *bottom*).

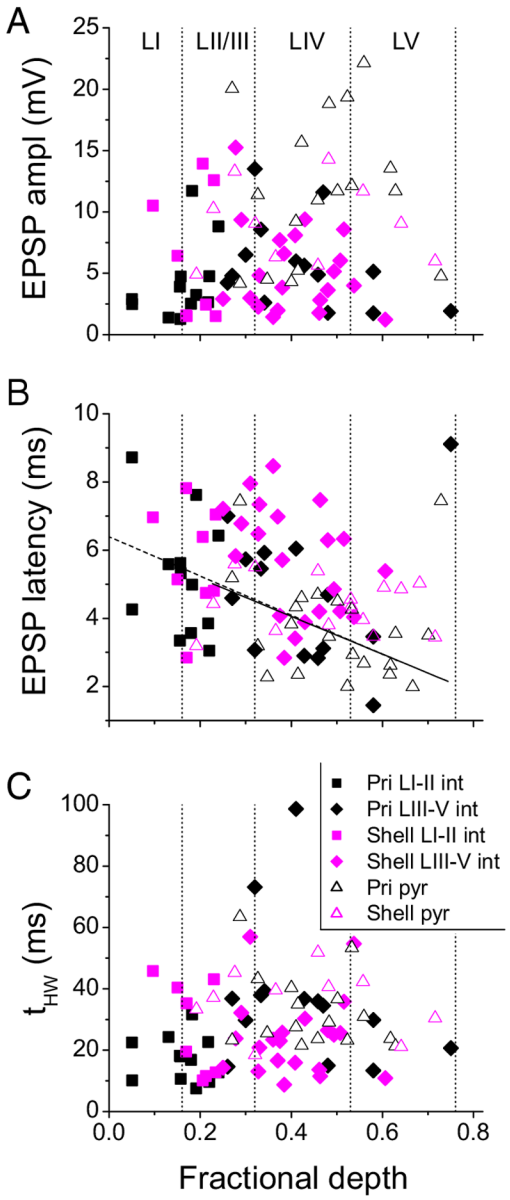

FIG. 4.

Variation in EPSP amplitude (*A*), mean latency (*B*), and duration (t_{HW}; *C*) with cortical depth for interneurons (closed symbols) and pyramidal cells (open triangles) from primary slices (black) and from shell slices (magenta). Depth was normalized to the distance in each slice from the pia to the white matter. There was no significant correlation for any parameter for either cell type except for mean latency in primary interneurons (*B*, dashed line; r =-0.504, $P < 0.05$) and primary pyramidal cells (*B*, solid line; r = -0.522, $P < 0.05$). Vertical dotted lines, boundaries of the cortical layers as indicated in *A*.

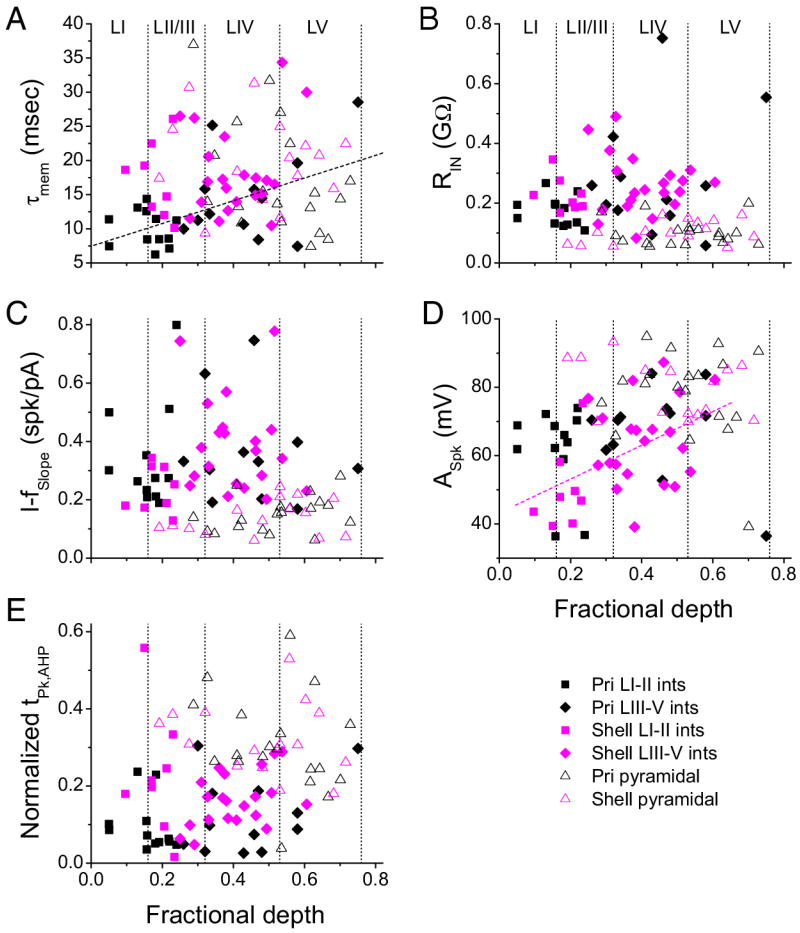

FIG. 5.

Variation in estimated membrane time constant (*A*), estimated resting input resistance (*B*), slope of the current-spike frequency relationship (*C*), spike amplitude (*D*), and normalized time of AHP peak (*E*) with cortical depth for interneurons (closed symbols) and pyramidal cells (open triangles) from primary slices (black) and from shell slices (magenta). Depth was normalized to the distance in each slice from the pia to the white matter. There was no significant correlation for any parameter for either cell type except for τ_{mem} in primary interneurons (*A*, dashed line; $r = 0.555$, $P < 0.005$) and A_{Spk} in shell interneurons (*D*, dashed line; $r = -0.477$, $P < 0.01$). Vertical dotted lines, boundaries of the cortical layers as indicated in *A*.

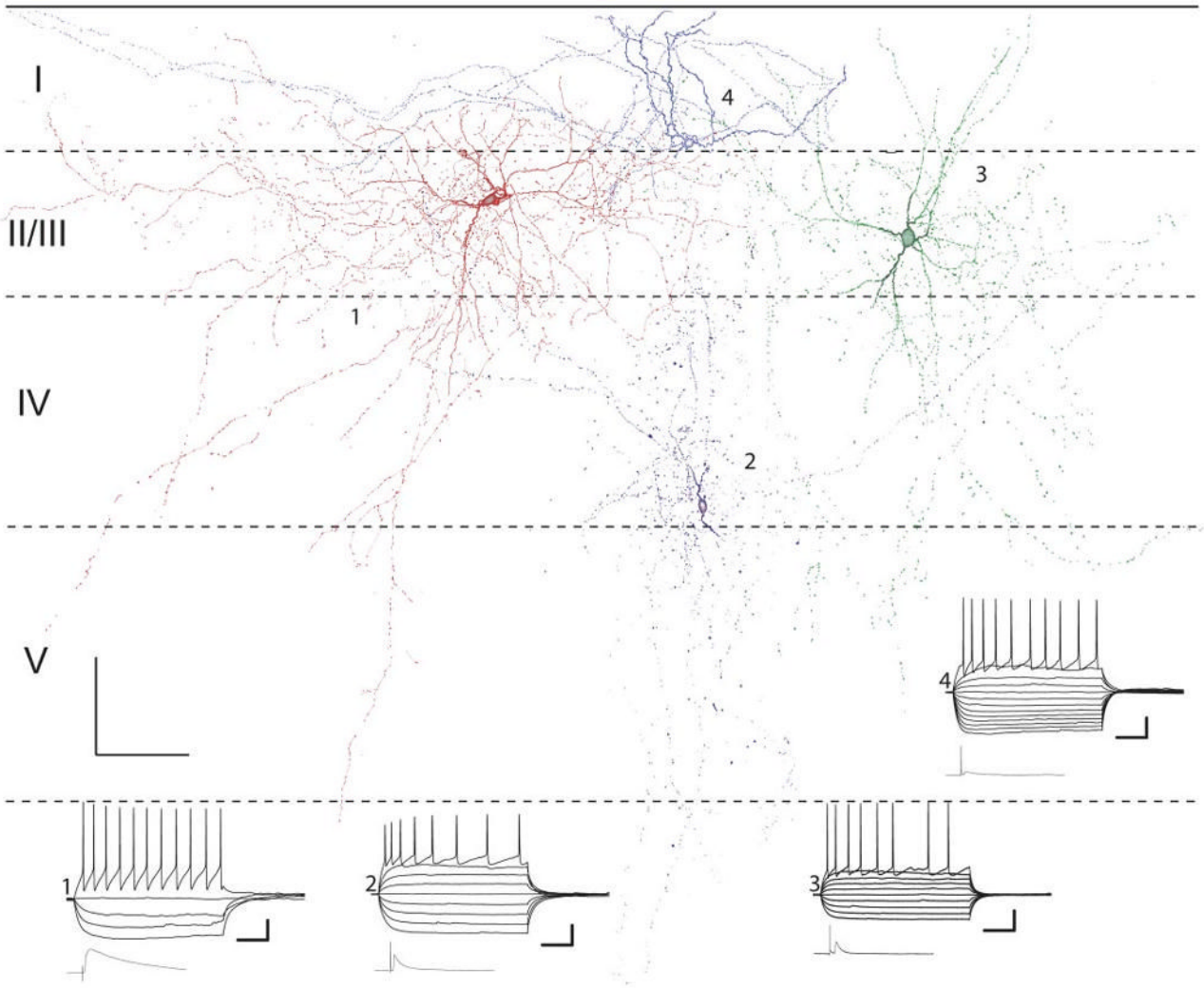

FIG. 6.

Camera lucida reconstructions of 4 interneurons in primary slices. Horizontal dashed lines, layer boundaries. Also shown are current clamp responses to polarizing current steps and mean maximal responses to TC stimulation (*bottom left*). Physiology traces and cells are numbered, starting with the red cell in layer II (1) and proceeding counterclockwise with the blue cell in layer I being number 4. Resting potentials (clockwise, from *top*): -72.4, -69.1, -75.0, and -70.9 mV. Current steps ranged from -200 to 0 pA for hyperpolarizing pulses and in increments of 75 pA until threshold. The pulse eliciting the superthreshold response varied between cells but was typically 375 pA. Scale bars: 100 μm, 100 μm (anatomy figure), 50 ms, 20 mV (current pulse responses), 25 ms, 6 mV (TC stim responses).

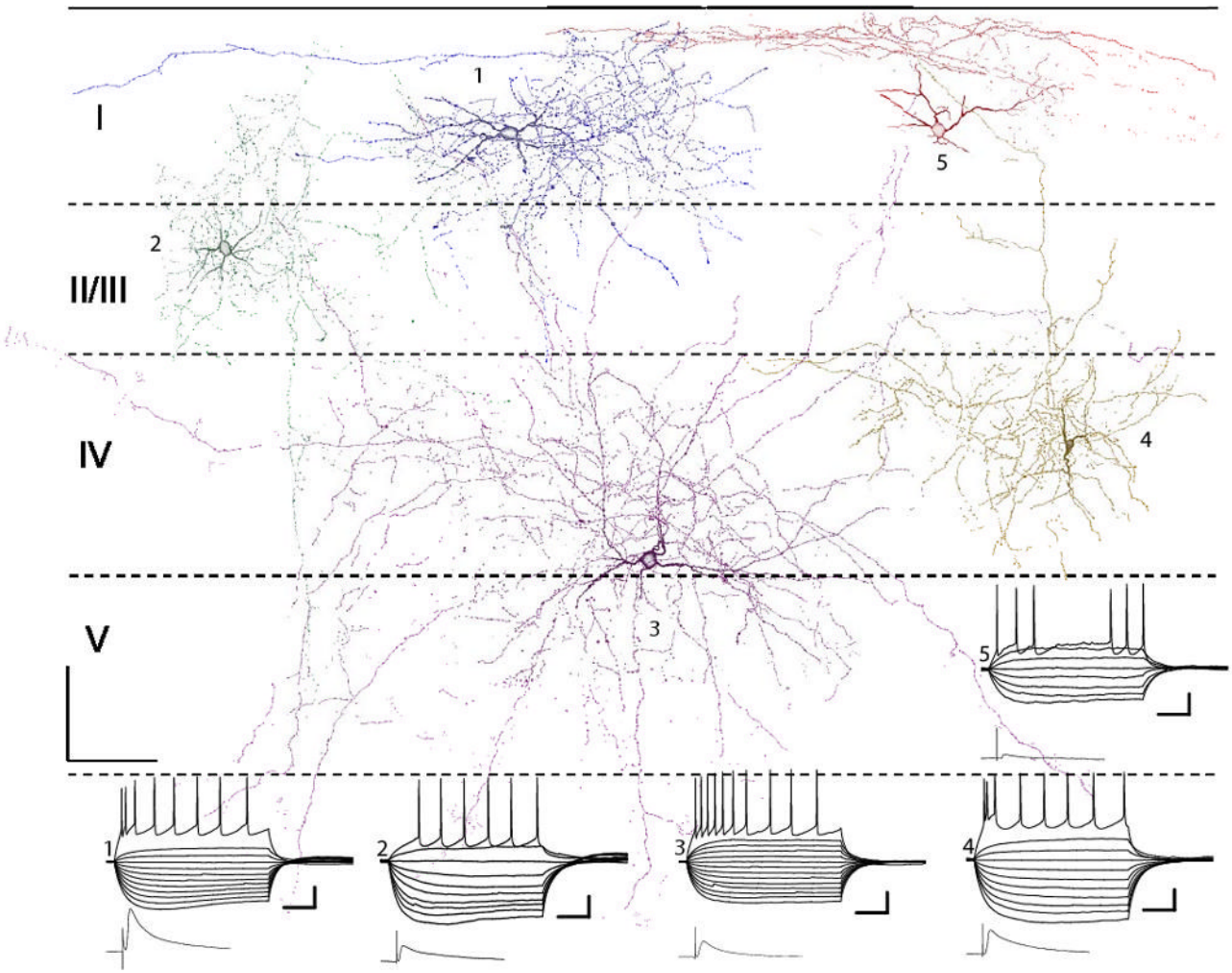

FIG. 7.

Camera lucida reconstructions of 5 interneurons in shell slices. Horizontal dashed lines, layer boundaries. Also shown are current-clamp responses to polarizing current steps and mean maximal responses to TC stimulation (*bottom left*). Physiology traces and cells are numbered, starting with the blue cell in layer I (1) and proceeding counterclockwise with the red cell in layer I being number 5. Resting potentials: 1, -73.6 mV; 2, -66.4 mV; 3, -73.3 mV; 4, -68.5 mV; and 5, -70.4 mV. Current steps ranged from -200 to 0 pA for hyperpolarizing pulses and in increments of 75 pA until threshold. The pulse eliciting the superthreshold response varied between cells but was typically 375 pA. Scale bars: 100 μm, 100 μm (anatomy figure), 50 ms, 20 mV (current pulse responses), 25 ms, 6 mV (TC stim responses).

TABLE 1

Comparison of intrinsic membrane and firing properties in layer 1 cells from transgenic (n = 13) vs. wild-type (n = 130) mice

Parameter	Animal	Mean ± SD	*P* Value
E_{Rest}, mV	GAD-GFP	-63.4 ± 2.63	0.0710
	Wild type	-61.7 ± 5.76	
τ_{mem}, ms	GAD-GFP	10.9 ± 4.86	0.8624
	Wild type	11.2 ± 5.30	
R_{UI}, Gω	GAD-GFP	0.186 ± 0.0667	0.5492
	Wild type	0.163 ± 0.135	
$I\text{-}V_{Slope\ ratio}$	GAD-GFP	1.09 ± 0.0877	0.5528
	Wild type	1.10 ± 0.0864	
V_{Thresh}, mV	GAD-GFP	27.2 ± 1.41	0.8224
	Wild type	26.4 ± 2.16	
$I\text{-}F_{Slope}$, spk/pA	GAD-GFP	0.334 ± 0.156	0.3338
	Wild type	0.291 ± 0.151	
ISI_{Ratio}	GAD-GFP	0.554 ± 0.306	0.4506
	Wild type	0.641 ± 0.399	
$I_{HW,spk}$, ms	GAD-GFP	0.703 ± 0.175	0.3011
	Wild type	0.780 ± 0.261	
A_{Spl}, mV	GAD-GFP	58.2 ± 12.7	0.1284
	Wild type	63.5 ± 11.7	
t_{pk},AHP	GAD-GFP	0.149 ± 0.138	0.5938
	Wild type	0.164 ± 0.0905	
A_{AHP}, mV	GAD-GFP	12.5 ± 2.03	0.02617
	Wild type	10.6 ± 2.89	

Parameter values were compared using unpaired Student's *t*-tests, with a significance level of 0.005 to correct for multiple comparisons.

TABLE 2

Properties of synaptic responses to stimulation of thalamic afferents in cells in auditory thalamocortical slices

	n	Lat_{Mo}, ms	A_{EPSP}, mV	$t_{HW.EPSP}$ ms
All interneurons	55	5.33±1.77*	5.26±3.73*	26.1±16.9*
All pyramid cells	27	4.01±1.30	10.5±5.74	34.8±15.8
LI & II primary interneurons	12	5.20±1.75	4.20±3.10§	17.1±7.28,†§
LIII-V primary interneurons	14	4.67±2.03	5.63±3.55*	36.9±23.3
LI & II shell interneurons	8	5.72±1.63*	6.31±5.33*	27.3±15.3
LIII-V shell interneurons	21	5.70±1.62*	5.23±3.51*	24.2±12.8
Primary pyramidal cells	17	3.77±1.55	11.7±5.96	35.8±17.6
Shell pyramidal cells	10	4.40±0.796	9.05±3.33	36.0±10.4

Values are means ± SD.

* Significantly different from primary pyramidal cells, Student's *t*-test, $P < 0.0167$. There was a significant effect of cell type on all three parameters [1-way ANOVA, LatMn:$F(5.81)=4.002$. $P < 0.01$: AEPSP:$F(5.81)=6.748$. $P < 10^{-4}$: $t_{HW\ EPSP}$:$F(5.81)=3.556$. $P <0.01$]. Other symbols indicate statistically significant differences between groups as assayed by Bonferoni's or Dunnett's T-3 post-hoc tests ($P < 0.05$):

† different from primary LIII-V interneurons;

≠ different from shell pyramidal cells;

§ different from primary and shell pyramidal cells.

TABLE 3

Intrinsic membrane and tiring properties of cells in auditory thalamocortical slices

	τ mem, msec[a]	R_{IN} GΩ[a]	I-$V_{Slope\ ratio}$	V_{Thresh} mV	I-F_{Slope}, spk/pA[a]	ISI_{Ratio}	$t_{HW,\ spk}$, msec	A_{Spk}, mV[a]	tPK_AHP[a]	A_{AHP}, mV
LI & II Primary ±interneurons	10.0±2.64[cd]	0.171 ±0.0497[ce]	1.07±0.059	-37.1 ±5.75	0.343 ±0.178[c]	0.708 ±0.300	0.636 ±0.137	61.7 ±12.5be	0.0954 ±0.0680[e]	14.2 ±2.70
LIII-V Primary interneurons	14.9±6.58	0.286 ±0.200[e]	1.07±0.105	-38.6 ±5.53	0.318 ±0.227[e]	0.615 ±0.346	0.636 ±0.267	67.6 ±13.1	0.125 ±0.0988[e]	14.9 ±4.49
LI & II shell interneurons	17.1±5.5	0.228 ±0.0583[e]	1.11±0.120	-35.2 ±7.03	0.237 ±0.0801[c]	0.442 ±0.314	0.834 ±0.186	50.1 ±11.8[e]	0.230±0.163	11.2 ±1.75
LIII-V shell interneurons	18.3±6.41	0.261 ±0.099[e]	1.17±0.129	-36.3 ±5.08	0.387 ±0.162[e]	0.576 ±0.306	0.694 ±0.197	64.2 ±12.5[e]	0.164 ±0.0692[e]	13.4 ±3.87
Primary pyramidal cells	16.6±7.94	0.0990 ±0.0421	1.11±0.107	-35.8 ±6.54	0.151 ±0.0571	0.676 ±0.313	0.747 ±0.264	79.5 ±13.2	0.319±0.124	12.6 ±2.22
Shell pyramidal cells	19.8±6.18	0.102 ±0.0391	1.12 ±0.0562	-38.2 ±2.64	0.138 ±0.0589	0.713 ±0.289	0.795 ±0.201	80.8 ±9.44	0.323 ±0.0904	12.1 ±2.18

Parameters were measured from responses to hyper-and depolarizing current pulses. Firing properties were measured from the response to the current pulse eliciting a train of spikes with firing frequency closest to 25 Hz. Spike and after hyper polarization shape parameters are averages over all spikes in this train.

[a] Significant effect of cell classification factor by one-way ANOVA.τ_{mem}:F(5.81)=3.798. P < 0.01: RIN:F(5,81)=11.85. P < 107: I-F_{Slope}:F(5, 81)=10.03, P < 10^{-6}: A_{Spk}:F(5, 81)=11.4, P < 10^{-7};$t_{Pk,AHP}$:F(5, 81)=14.2, P < 109. Other symbols indicate statistically significant differences between groups as assayed by Bonferoni's or Dunnett's T-3 post hoc tests (P <0.05):

[b] different from primary LIII-V interneurons:

[c] different from shell LIII-V interneurons:

[d] different from shell pyramidal cells:

[e] different from primary and shell pyramidal cells.